ACS APPLIED MATERIALS & INTERFACES

Research Article

Cite This: ACS Appl. Mater. Interfaces 2017, 9, 44392−44401

www.acsami.org

Supramolecular Nanomedicine Constructed from Cucurbit[8]uril-Based Amphiphilic Brush Copolymer for Cancer Therapy

Dan Wu,[†] Yang Li,[†] Jie Yang,[‡] Jie Shen,[§] Jiong Zhou,[‡] Qinglian Hu,[∥] Guocan Yu,*[,‡,⊥] Guping Tang,*[,†] and Xiaoyuan Chen*[,⊥]

[†]Institute of Chemical Biology and Pharmaceutical Chemistry, Department of Chemistry, and [‡]State Key Laboratory of Chemical Engineering, Center for Chemistry of High-Performance & Novel Materials, Department of Chemistry, Zhejiang University, Hangzhou 310027, P. R. China

[§]School of Medicine, Zhejiang University City College, Hangzhou 310015, P. R. China

[∥]College of Biotechnology and Bioengineering, Zhejiang University of Technology, Hangzhou 310014, P. R. China

[⊥]Laboratory of Molecular Imaging and Nanomedicine, National Institute of Biomedical Imaging and Bioengineering, National Institutes of Health, Bethesda, Maryland 20892, United States

Supporting Information

ABSTRACT: An amphiphilic supramolecular brush copolymer CB[8]⊃(PEG-Np·PTPE) was constructed on the basis of a novel host−guest molecular recognition model formed by cucurbit[8]uril (CB[8]), 4,4′-bipyridinium derivative, and PEGylated naphthol (PEG-Np). In aqueous solution, the resultant supramolecular brush copolymer self-assembled into supramolecular nanoparticles (SNPs), by which the anticancer drug doxorubicin (DOX) was encapsulated in the hydrophobic core, establishing an artful Förster resonance energy transfer system with dual fluorescence quenched. With the help of intracellular reducing agents and low pH environment, the SNPs disassembled and the loaded drug molecules were released, realizing in situ visualization of the drug release via the location and magnitude of the energy transfer-dependent fluorescence variation. The cytotoxicity evaluation indicated DOX-loaded SNPs effectively inhibited cell proliferation against HeLa cells. Animal experiments demonstrated that these DOX-loaded SNPs highly accumulated in tumor tissues through the enhanced permeability and retention effect and also had a long blood circulation time. These multifunctional supramolecular nanoparticles possessing self-imaging and controllable drug release ability exhibited great potential in cancer therapy.

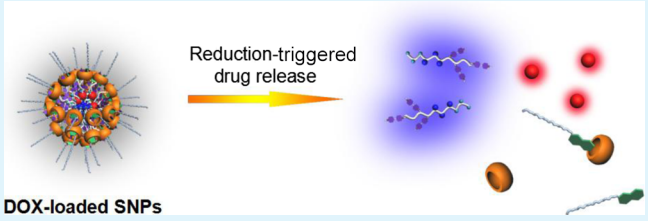

KEYWORDS: *supramolecular chemistry, host−guest system, aggregation-induced emission, drug delivery, self-assembly*

1. INTRODUCTION

The goals of advanced nanomedicines seek ways to address various shortcomings and challenges faced by conventional medicines, including impaired target specificity, poor bioavailability, easy degradability, systemic toxicity, and so forth.[1−4] The employment of sophisticated drug delivery systems (DDSs) improves the delivery of chemotherapeutic drugs to the target locations, with control of their navigation in the body.[5−8] Among various DDSs, nanoparticles (NPs) constructed from polymeric materials have become prominent in DDSs because of their excellent biocompatibility and biodegradability.[9−12] For example, poly(glycolic acid), poly(D,L-lactic acid), poly(D,L-lactic-coglycolic acid), poly(ethylene glycol) (PEG), and so forth have been widely applied to develop smart DDSs.[13,14] The first Food and Drug Administration approved nanomedicine, DOXIL, is a typical example by using amphiphilic 1,2-distearoyl-*sn*-glycero-3-phosphoethanolamine-conjugated PEG as a component of the drug (doxorubicin) carriers.[15−18] Currently, other polymeric NPs (NC6004, NK012, and NK105) constructed from PEG and polypeptide copolymers are also undergoing clinical trials.

However, the only mission of these conventional DDSs is to deliver therapeutic drugs. To trace the release and excretion of the nanomedicines when they enter the cells, it is necessary to develop visible delivery vehicles possessing self-imaging capability. For the most reported polymeric NPs, the building blocks are always amphiphilic block copolymers whose hydrophilic and hydrophobic segments are linked by non-cleavable covalent bonds. Complicated organic/polymeric synthesis or post modifications were demanded to incorporate multiple functions into the platforms. Furthermore, the encapsulated drugs are always released through diffusion because of covalent linkages between the building blocks, which are lack of stimuli-responsive capability, reducing drug accumulation at the site of action and thereby decreasing the anticancer efficacy. By sharp contrast, the dynamic and flexible nature of the noncovalent bonds grants the resultant supramolecular nanomaterials with tunable mechanical, chemical,

Received: November 3, 2017
Accepted: December 5, 2017
Published: December 5, 2017

DOI: 10.1021/acsami.7b16734
ACS Appl. Mater. Interfaces 2017, 9, 44392−44401

and biological characteristics, contributing distinct and useful properties that have not been realized in traditional polymeric NPs.[19−23] Among diverse noncovalent forces, such as metal-coordination, hydrophobic interactions, hydrogen bonding, van der Waals interactions, and $\pi-\pi$ interactions, host−guest interactions have successfully attracted scientists' attention owing to their affluent stimuli-responsive behaviors.[24−27] However, only very few examples have been reported by using host−guest recognition motifs to fabricate theranostic DDSs.[28−31]

Herein, we employed the CB[8]-based ternary host−guest molecular recognition motif to prepare an amphiphilic brush copolymer by utilizing CB[8], PTPE, and PEG-Np as the building blocks (Scheme 1a). In aqueous solution, the resultant

Scheme 1. (a) Chemical Structures of the Building Blocks (CB[8], PEG-Np, and PTPE) and the Preparation of SNPs from CB[8], PEG-Np, and PTPE; (b) Schematic Illustration of the Imaging-Guided Drug Delivery

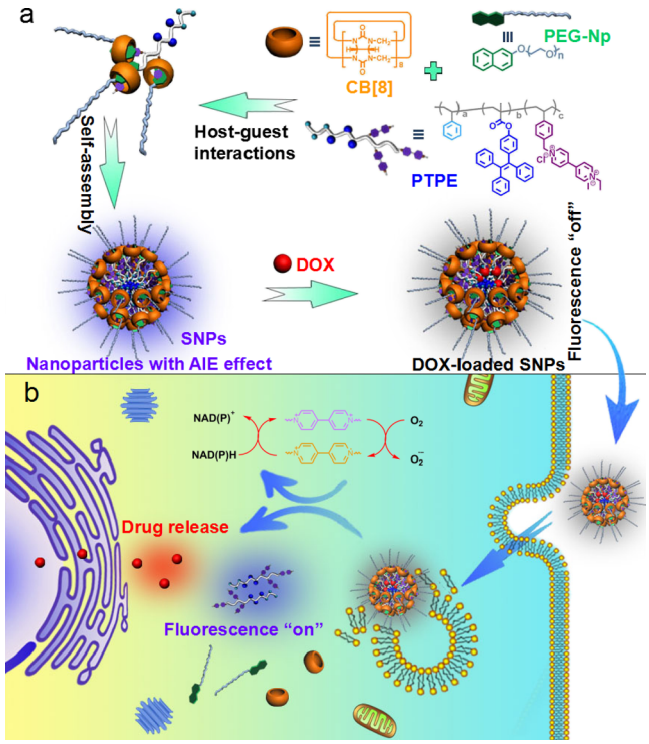

supramolecular brush copolymer self-assembles into supramolecular nanoparticles (SNPs), which can be used to encapsulate the anticancer drug doxorubicin (DOX) in its hydrophobic core, establishing a Förster resonance energy transfer (FRET) system, in which the tetraphenylethene (TPE) group acts as a donor and the drug molecule DOX acts as an acceptor.[32,33] When the DOX-loaded SNPs enter cells, with the help of intracellular reducing agents and low pH environment, they are disassembled and the loaded drug molecules are released. More excitingly, the energy transfer relay (ETR) between TPE groups and DOX is simultaneously interrupted,[34,35] and the "silenced" fluorescence is recovered, realizing in situ visualization of the drug release via the location and magnitude of the energy transfer-dependent fluorescence variation (Scheme 1b). In vitro and in vivo investigations reveal that reasonable integration of the functionalities mentioned above in one intelligent drug carrier enables integrated self-diagnosis treatment with excellent drug delivery and release abilities and minimizes nonspecific systemic distribution of the drugs, significantly enhancing the treatment efficiency while lowering the systemic toxicity.

2. RESULTS AND DISCUSSION

2.1. Preparation of the Amphiphilic Supramolecular Brush Copolymer. As an important member of the cucurbit[*n*]uril family, cucurbit[8]uril (CB[8]) is able to simultaneously encapsulate two guest molecules in its hydrophobic cavity, establishing a stable ternary host−guest complex.[36−38] For example, CB[8] can encapsulate the naphthol (Np) derivative and methyl viologen (PQ^{2+}) groups in its hydrophobic cavity to construct 1:1:1 complex CB[8]⊃(PQ^{2+}·Np), which is based on the host-enhanced charge-transfer (CT) interaction, where Np acts as the electron donor and PQ^{2+} acts as the electron acceptor in the cavity of CB[8].[39−41] Furthermore, reduction of PQ^{2+} into its radical form always leads to the dissociation of the ternary host−guest complexation,[42,43] thus a reduction-responsive host−guest complex can be constructed.[44] With respect to the distinct host−guest binding features, CB[8] is a suitable noncovalent linker to prepare supramolecular polymers, which can be possibly applied to construct smart DDSs. The host-enhanced charge-transfer interaction among CB[8], PEG-Np, and PTPE was studied by ^{1}H NMR spectroscopy. Because of the relatively low solubility of PTPE, viologens (PQ) were employed as a model molecule to study the host−guest interaction in water. Without CB[8], the resonance signals of the protons on PQ and PEG-Np resonated at basically the same positions as that observed in the ^{1}H NMR spectra of free PQ and PEG-Np (Figure 1c), indicating that no CT complex was generated under this condition. Nevertheless, upon addition of 1.0 equiv amount of CB[8] into the mixture, the signals of the aromatic protons (H_a and H_b) on the viologen residue upfield shifted dramatically. Meanwhile, the observation of the broadening effect was noticed as the resonance peaks corresponding to the protons H_{1-5} on PEG-Np disappeared after the complexation

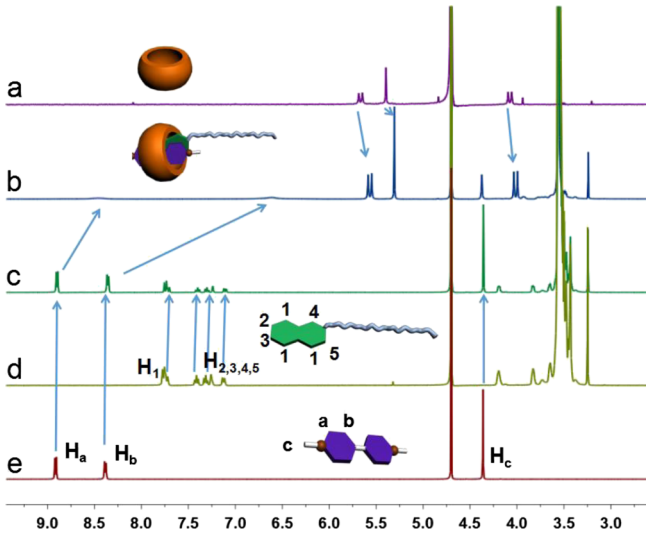

Figure 1. Partial ^{1}H NMR spectra (400 MHz, D_2O, 295 K): (a) CB[8] (1.00 mM). (b) Mixture of CB[8], PQ, and PEG-Np (molar ratio: 1:1:1, concentration: 1.00 mM). (c) Mixture of PQ and PEG-Np (molar ratio: 1:1, concentration: 1.00 mM). (d) PEG-Np (1.00 mM). (e) PQ (1.00 mM).

DOI: 10.1021/acsami.7b16734
ACS Appl. Mater. Interfaces 2017, 9, 44392−44401

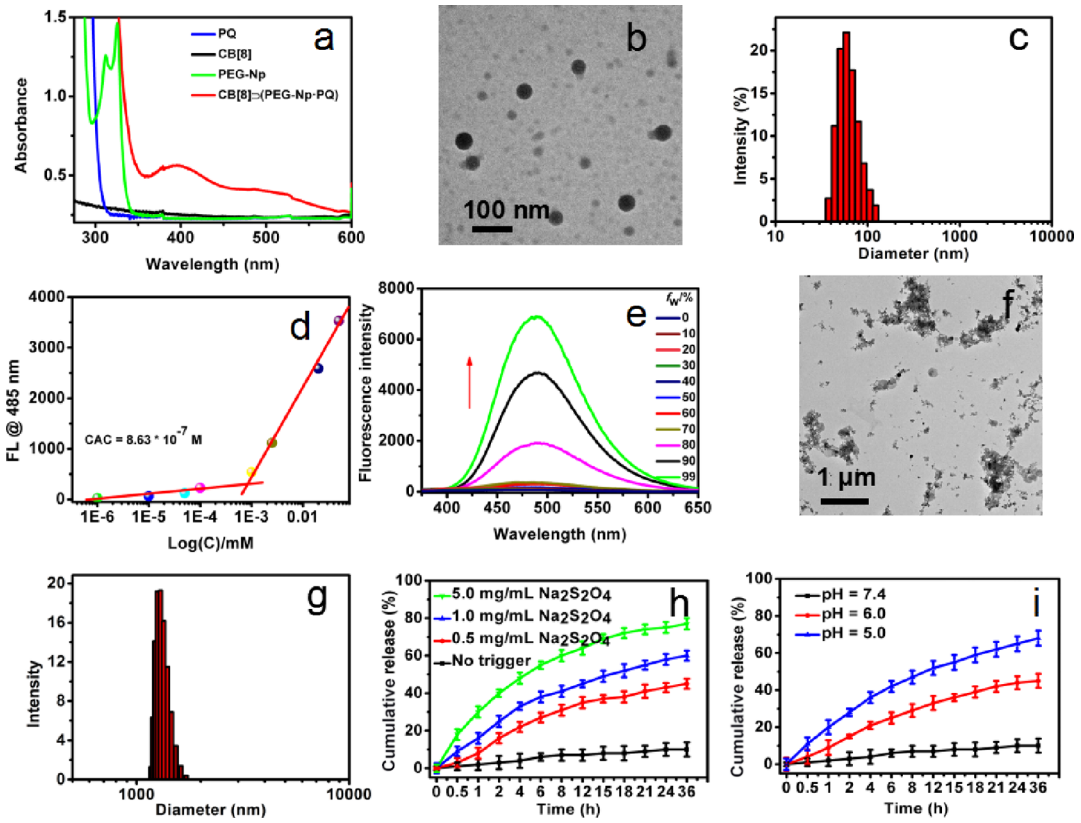

Figure 2. (a) UV−vis spectra of PQ, PEG-Np, CB[8], and CB[8]⊃(PEG-Np·PQ) (molar ratio = 1:1:1) at the concentration of 1.00 mM in water. (b) TEM image of SNPs self-assembled from CB[8]⊃(PEG-Np·PTPE). (c) DLS result of SNPs self-assembled from CB[8]⊃(PEG-Np·PTPE). (d) Plots of the fluorescence (FL) intensity at 485 nm vs the concentration of CB[8]⊃(PEG-Np·PTPE). (e) Fluorescence spectra of CB[8]⊃(PEG-Np·PTPE) in THF/H_2O mixtures with different f_w values. (f) TEM image of SNPs in the condition of 1.00 mg/mL $Na_2S_2O_4$. (g) DLS result of SNPs in the condition of 1.00 mg/mL $Na_2S_2O_4$. (h) Drug release curves of DOX-loaded SNPs in the aqueous solution containing different amounts of $Na_2S_2O_4$. (i) Drug release curves of DOX-loaded SNPs under different pH values.

(Figure 1b).[45] We could speculate that CB[8] mediates the construction of a stable CT complex between the alkoxynaphthalene and viologen residues of PEG-Np and PQ, forming a well-defined CB[8]⊃(PEG-Np·PQ) complex.

Further proof for the generation of the CB[8]⊃(PEG-Np·PQ) complex was acquired from UV spectroscopy. Upon mixing CB[8], PQ, and PEG-Np (molar ratio = 1:1:1), an orange-yellow solution formed immediately, demonstrating the generation of a CT complex (Figure S4).[46,47] Figure 2a shows the characteristic charge-transfer band ranging from 400 to 600 nm developed by adding of CB[8] into the aqueous solution containing PQ and PEG-Np. Without CB[8], the charge-transfer band was undetectable (Figure S5), further demonstrating that CB[8] plays a significant role in the generation of the ternary complex.

With respect to the establishment of the CB[8]⊃(PEG-Np·PQ), CB[8] was employed as an desired noncovalent linker to prepare an amphiphilic supramolecular brush copolymer CB[8]⊃(PEG-Np·PTPE) by using CB[8], PTPE, and PEG-Np as the building blocks, where the PEG segments acted as the hydrophilic part and the backbone of PTPE acted as the hydrophobic part. In an aqueous solution, CB[8]⊃(PEG-Np·PTPE) could self-assemble into SNPs. Dynamic light scattering (DLS) and transmission electron microscopy (TEM) studies were performed to study the size and morphology of these SNPs.[48] As shown in the TEM image (Figure 2b), the diameters of spherical particles were about 40 nm, in agreement with the result of DLS measurement (Figure 2c), which showed a main size of 63 nm. Notably, the diameter of the particles acquired from the TEM image was slightly smaller than the data measured by DLS, which was ascribed to the swelling effect of aggregates in aqueous solution. The self-assembly of the amphiphilic supramolecular brush copolymer CB[8]⊃(PEG-Np·PTPE) in water was also investigated using the concentration-dependent fluorescence. As shown in Figure 2d, the critical aggregation concentration (CAC) of CB[8]⊃(PEG-Np·PTPE) was determined to be 8.63×10^{-7} M, which was notably higher than the result of PTPE (Figure S6), owing to the introduction of hydrophilic PEG segments through host−guest complexation. The fluorescence of the solution was weak when its concentration was lower than the corresponding CAC value. However, the fluorescence intensity increased rapidly as the concentration increased higher than its CAC, attributing to the aggregation-induced emission (AIE) effect of gathering CB[8]⊃(PEG-Np·PTPE) SNPs. After formation of SNPs, the AIE behavior of PTPE was first evaluated. As shown in Figure 2e, PTPE emitted faint fluorescence when dissolved in tetrahydrofuran (THF), while the fluorescence intensity dramatically increased by increasing the water fraction (f_w) value. When the f_w got to 99 vol %, the fluorescence intensity of PTPE was 100 times more than in THF. All these results demonstrated that after the formation of CB[8]⊃(PEG-Np·PTPE), the AIE property of the TPE residue of PTPE was effectively maintained.

Under the reductive conditions, viologens could be reduced to the relevant cationic radical state, leading to the disassembly

DOI: 10.1021/acsami.7b16734
ACS Appl. Mater. Interfaces 2017, 9, 44392−44401

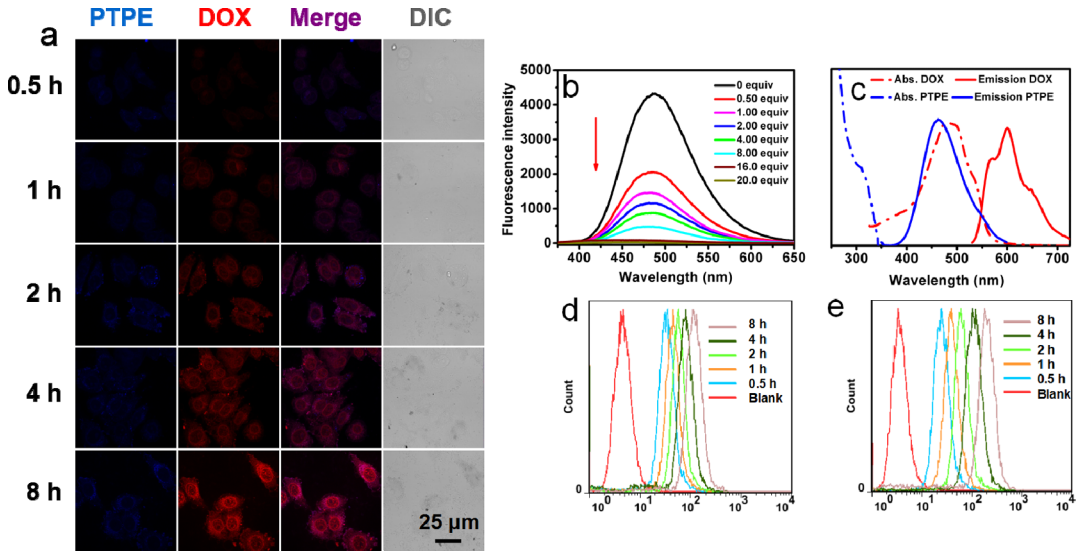

Figure 3. (a) Confocal laser scanning microscopy images of the HeLa cells exposed to DOX-loaded SNPs for various time periods. Scale bars = 25 μm. (b) Fluorescence spectra of SNPs self-assembled from CB[8]⊃(PEG-Np·PTPE) in the presence of different amounts of DOX. (c) UV−vis and fluorescence spectra of PTPE and DOX. Flow cytometry results of fluorescence signals in HeLa cells exposed to DOX·HCl (d) and DOX-loaded SNPs (e) for different times. The DOX concentration was 5.00 μM.

of the SNPs from the CB[8]⊃(PEG-Np·PTPE) complex.[49−52] As can be seen in Figure 2f, the SNPs disassembled into irregular aggregates in the presence of $Na_2S_2O_4$ (1.00 mg/mL). In this process, the solution turned to be cloudy caused by the precipitation of PTPE from the solution, confirming the disassociation of the CB[8]⊃(PEG-Np·PTPE) complex by $Na_2S_2O_4$. Furthermore, the DLS measurements were also conducted to study the reduction-induced disassembly process. The average diameter of the nanoparticles varied from 63 nm to 1.4 μm after culturing the SNPs with an aqueous solution containing $Na_2S_2O_4$ (1.00 mg/mL) for 24 h (Figure 2g), which was consistent with the result obtained from TEM studies.

2.2. Drug Release Investigations and Establishment of the Förster Resonance Energy Transfer System. The hydrophobic pocket of the SNPs was employed to load the hydrophobic anticancer drug DOX. After DOX was deprotonated by triethylamine, it was successfully loaded into the hydrophobic core of the SNPs. On the basis of the standard curve, the drug loading content was calculated to be 11.7%, suggesting that this supramolecular vector was a suitable platform to load the hydrophobic anticancer drug. As discussed above, the reduction-triggered disassembly of the SNPs could be utilized to control the drug release behavior. The release behavior of DOX-loaded SNPs was first investigated in the aqueous solution containing $Na_2S_2O_4$ (Figure 2h). Only 10% DOX was released within 36 h without stimulus attributing to the $\pi-\pi$ stacking and hydrophobic interactions between DOX and PTPE. However, a much faster release of DOX emerged upon addition of $Na_2S_2O_4$ into the DOX-loaded SNPs solution. For example, in the presence of $Na_2S_2O_4$ from 0.5 to 5.0 mg/mL, the release amount gradually increased from 45 to 77% within 36 h, demonstrating that the reduction-triggered dissociation of the supramolecular complex indeed caused the controlled drug release.

The release behavior of DOX-loaded SNPs was also monitored in the aqueous solution at different pH values. As shown in Figure 2i, by decreasing the solution pH values, DOX was greatly released from the SNPs, i.e., 45% release efficiency at pH 6.0 and 68% at pH 5.0 within 36 h. Because the microenvironment of tumor is slightly acidic, the DOX release from DOX-loaded SNPs can be triggered rapidly, which plays an important role in chemotherapy. This pH-triggered drug release behavior can be reasonably explained by the protonation of DOX in acidic environments that promoted the escape of water-soluble DOX·H^+ from the hydrophobic core of SNPs, making DOX-loaded SNPs an ideal candidate for drug delivery.[53−55]

To trace the release and excretion of the nanomedicines, it is urgent to develop self-imaging drug carriers, especially with "turn on" fluorescence.[56−61] Interestingly, we found that upon formation of DOX-loaded SNPs, the fluorescence intensity of PTPE decreased dramatically (Figure 3b). The decrease in the fluorescence intensity of PTPE in SNPs was attributed to FRET. As shown in Figure 3c, there was an overlap in the emission spectrum of PTPE and the absorption spectrum of DOX, hence the emitted fluorescence from PTPE could be absorbed by DOX. Moreover, the fluorescence intensities of DOX and PTPE recovered effectively once DOX was released (Figures S7 and S8), as the energy transfer relay effect between PTPE and DOX was interrupted. The fluorescence variation may be proposed as follows: when the supramolecular brush copolymer aggregated, the TPE moieties and DOX coexisted in the hydrophobic core of the SNPs. Meanwhile, the short distance between TPE and DOX promoted the occurrence of FRET. Therefore, the fluorescence of both TPE and DOX was quenched through ETR, in which the emission from TPE transferred to DOX, which was further self-quenched because of the aggregation-caused quenching (ACQ) effect of DOX.

Considering the possible applications of CB[8]⊃(PEG-Np·PTPE) SNPs in drug delivery, the 3-(4′,5′-dimethylthiazol-2′-yl)-2,5-diphenyl tetrazolium bromide (MTT) assay was used to evaluate their cytotoxicity. As shown in Figure S9, even if the concentration of CB[8]⊃(PEG-Np·PTPE) SNPs reached up to 200 μg mL^{-1}, the cell survival rates were still higher than 70%, indicating low cytotoxicity of these SNPs. To study the internalization and drug release profile of DOX-loaded SNPs in vitro, we incubated the DOX-loaded SNPs with HeLa cells and monitored the intracellular changes in the fluorescence signal

DOI: 10.1021/acsami.7b16734
ACS Appl. Mater. Interfaces 2017, 9, 44392−44401

over extended periods of time (0.5−8 h) using confocal laser scanning microscopy (CLSM). As can be seen in Figure 3a, the blue fluorescence arising from PTPE co-localized with the red fluorescence related to DOX in the cytoplasm at 0.5 h, which suggested PTPE and DOX still aggregated together in SNPs in the cells. Over time, the red fluorescence intensity increased, indicating that DOX was gradually released from SNPs in a time-dependent manner. When the incubation time extended to 2 h, strong red fluorescence corresponding to DOX appeared in the cell nucleus in which DOX performed its anticancer activities. By further extending incubation time to 8 h, most of the DOX molecules were translocated into the cell nucleus. It should be noted that PTPE still dispersed in cell plasma and there was no blue signal in the cell nucleus. By tracing the spatial and temporal variation of the different signals in DDSs, we could conclude that SNPs were first internalized by cells and then transported into endosomes/lysosomes, in which DOX dissociated from SNPs owing to the weakly acidic environment and reducing environment. The released DOX then entered and lit up the nucleus, whereas PTPE remained in the cytoplasm. As a result, the ETR effect between PTPE and DOX was interrupted and the ACQ effect of DOX was relieved, then the fluorescence of both PTPE and DOX was waken up, and the dual-fluorescence quenched DDS converted into a dual-fluorescence emissive DDS.

The internalization of DOX was further quantified by flow cytometry. As can be seen in Figure 3e, the endocytosis of DOX-loaded SNPs by HeLa cells was time-related. With the extension of culture time, the intracellular DOX concentration increased rapidly. From Figure 3d,e, we also knew that the internalization of DOX-loaded SNPs was comparable to DOX·HCl under the same conditions. The cytotoxicity of DOX·HCl and DOX-loaded SNPs toward HeLa cells were also assessed by the MTT assay. After 24 or 48 h incubation, the cell survival rate was examined. As shown in Figures S10 and S11, DOX-loaded SNPs showed high cytotoxicity similar to DOX·HCl at a high DOX concentration, which indicated that the anticancer efficacy of the loaded DOX was kept efficiently after encapsulation by the SNPs. All these results manifested that such SNPs were highly effective in transporting DOX into cancer cells and performing therapeutic effect.

2.3. In Vivo Drug Delivery and Antitumor Treatment.

It has been demonstrated that nanomedicine could enhance the treatment effects of hydrophobic small molecule drugs by improving their pharmacokinetics. On account of this, we investigated whether SNPs were able to prolong the blood circulation time of DOX and deliver more DOX into the tumor tissues. The plots of the plasma concentration of DOX·HCl and DOX-loaded SNPs versus time were presented in Figure 4a. The clearance of free DOX·HCl from body was extremely fast, its blood circulation time was much shorter than that of DOX-loaded SNPs. Meanwhile, the mice administrated with DOX-loaded SNPs had a greater area under the curve (4.18 h·mg·mL^{-1}) than the DOX·HCl-treated group (0.91 h·mg·mL^{-1}). The reason was that the PEGylation on SNPs effectively hindered secondary interactions between proteins and SNPs, preventing their elimination by the reticuloendothelial system, which is beneficial for prolonging the drug circulation time.[62,63]

To further confirm whether the DOX-loaded SNPs could enhance the delivery of DOX to tumor sites by the enhanced permeability and retention (EPR) effect,[64,65] the Balb/c mice bearing HeLa tumor were treated with DOX-loaded SNPs via tail vein injection (5.00 mg DOX/kg) to monitor the

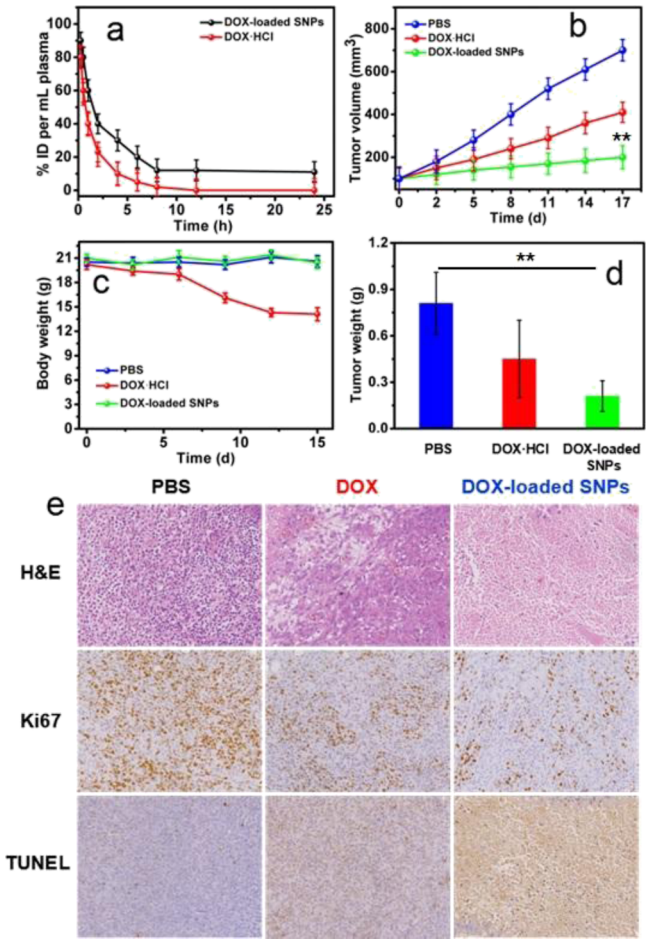

Figure 4. (a) Curves of the plasma concentration of DOX in DOX·HCl and DOX-loaded SNPs groups vs time after i.v. injection (5.00 mg/kg) (n = 3). (b) Curves of the tumor volume vs time after different treatments (n = 7). (c) Changes in the body weight after various treatments (n = 7). (d) Mean weights of tumors after different treatments (n = 7, $^{**}p < 0.01$). (e) Histological studies of tumor tissues after various formulations.

biodistribution of DOX. Mice injected with DOX·HCl were marked as the control group. After 24 h injection, ex vivo fluorescence imaging of tumor tissues and major internal organs were performed and are shown in Figure S12. There was no apparent fluorescence localization in the corresponding regions of mice that received free DOX·HCl because the small-molecular drug DOX·HCl was easily cleared from the body. However, comparing with DOX·HCl-treated group, the DOX-loaded SNPs-treated group had stronger fluorescence, owing to the prolonged circulation time of the DOX-loaded SNPs in the physiological environment and higher tumor accumulation benefiting from the EPR effect. A single dose of free DOX·HCl and DOX-loaded SNPs was intratumorally injected into the tumor tissue to further demonstrate that the DOX-loaded SNPs can effectively reside within the tumor (Figure S13). At the very beginning, the mice injected with DOX·HCl and DOX-loaded SNPs exhibited strong fluorescence signals at the tumor site. It was worthy pointing out that the fluorescence intensity in the tumor region quickly weakened and finally diminished after 8 h post injection for the mice administrated with DOX·HCl, which was ascribed to the fast clearance of free DOX·HCl. By marked contrast, the fluorescence at the tumor site was always at the steady state during the whole experimental period for the

DOI: 10.1021/acsami.7b16734
ACS Appl. Mater. Interfaces 2017, 9, 44392−44401

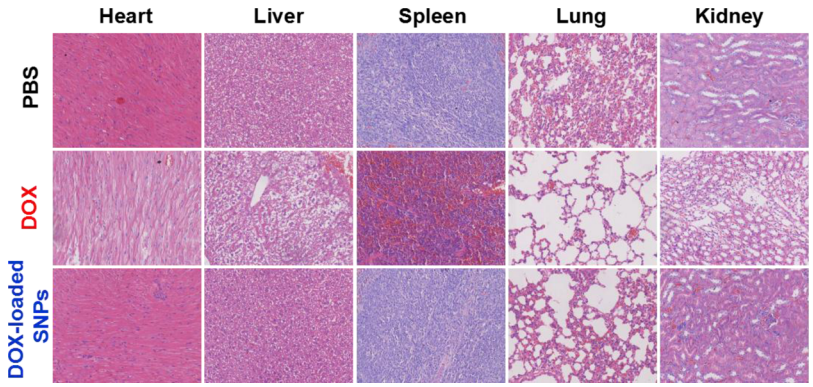

Figure 5. H&E staining of the major internal organs separated from the mice injected with PBS, DOX·HCl, and DOX-loaded SNPs.

DOX-loaded SNPs-treated mice, suggesting that supramolecular nanocarriers had a better tumor accumulation than DOX·HCl, which was crucial for suppression of tumor growth in a long period of treatment.

Encouraged by the former excellent performances of DOX-loaded SNPs, we proceeded to evaluate the antitumor effect on a HeLa tumor model. While the tumor size grew up to about 100 mm^3, the mice bearing HeLa tumor were randomly assigned into three groups: (i) phosphate-buffered saline (PBS), (ii) free DOX·HCl, and (iii) DOX-loaded SNPs. As can be seen in Figure 4b, the tumor volume exhibited a rapid increase in the PBS group. Compared with the control group, the mice injected with DOX·HCl exhibited a moderate tumor inhibition. What's exciting was that treatment with DOX-loaded SNPs as a chemotherapeutic agent could inhibit tumor growth significantly, and the tumor volume was far lower than the size in the DOX·HCl-treated group on the 15th day. The excellent tumor inhibitory effect of DOX-loaded SNPs was further proved by the tumor photos (Figure S15) and tumor weights (Figure 4d). All these in vivo experimental results and analysis suggested that the DOX-loaded SNPs could be effectively delivered to the tumor tissue by taking advantage of the EPR effect and perform a sustained release of the encapsulated DOX in the tumor to effectively inhibit tumor growth.

Hematoxylin and eosin (H&E), terminal deoxynucleotidyl transferase dUTP nick end labeling (TUNEL), and Ki67 staining of tumor slices harvested after treatment were further carried out to reveal the therapeutic efficacy. Histological examination revealed extensive karyopyknosis and necrosis in the tumors collected from the DOX·HCl group, whereas tumors from the other two groups were more viable (Figure 4e), demonstrating the excellent therapeutic efficacy of SNPs. Meanwhile, in comparison with those in the PBS- or DOX·HCl-treated groups (Figure 4e), administration of DOX-loaded SNPs greatly increased the percentage of apoptotic cells in TUNEL staining and decreased the number of proliferating cells in the Ki67 staining assay. All of these results suggested that DOX-loaded SNPs improved the efficacy of treatment in inducing apoptosis and inhibiting proliferation of tumor cells.

Systemic toxicity evaluation of the drug vehicles is a crucial factor for preclinical evaluation. The changes in the body weight of mice are usually evaluated to indicate the systemic toxicity. Throughout the process of treatment, the mice injected with PBS or DOX-loaded SNPs behaved normally, and no noticeable fluctuation in the body weight was detected (Figure 4c), indicating that the DOX-loaded SNPs exhibited relatively low systemic toxicity. On the contrary, significant decrease in body weight was observed in the mice injected with DOX·HCl, indicating that remarkable side effects were caused by DOX·HCl. In addition, the average lifespans of the mice in PBS and DOX·HCl groups were obviously shorter than that treated with DOX-loaded SNPs (Figure S14), suggesting that the antitumor performance of DOX·HCl was relatively poor.

The outstanding therapeutic performance with negligible side effects was further verified by histopathological analysis of tissue sections stained with H&E.[66−68] As shown in Figure 5, swollen muscle fiber cells in the heart were observed in the DOX·HCl-treated group, while no visible heart damage was detected in the other groups. Meanwhile, histological analysis of other organ slices of the mice treated with DOX·HCl showed structurally disordered renal tubules with pyknotic nuclei and without lumen, and prominent steatosis and necrosis in the hepatocytes. However, no obvious lesions could be found in the DOX-loaded SNP-treated group. The reduced toxicity of SNPs can be rationally explicated by the nano-composite structure, which was preferentially delivered to the tumor region, thus diminishing undesirable toxicity toward normal tissues. Collectively, these data indicated the superior safety and potency of the DOX-loaded SNPs for delivering theranostic agents in vivo.

3. CONCLUSIONS

In summary, a novel host−guest molecular recognition motif between cucurbit[8]uril (CB[8]), electron-deficient 4,4′-bipyridinium derivative (PQ), and electron-rich PEG-Np was utilized to construct an amphiphilic supramolecular brush copolymer CB[8]⊃(PEG-Np·PTPE), which was characterized with the AIE effect. In aqueous solutions, the resultant supramolecular brush polymer could self-assemble into SNPs, which acted as a supramolecular nanocarrier to encapsulate DOX to establish a self-imaging DDS. In the aggregation state, the fluorescence from both TPE and DOX was quenched by the combined action of the ETR and ACQ effects. However, with the help of intracellular reducing agents and low pH environment, self-imaging DDSs were disassembled and the loaded drug molecules were released. As a result, the energy transfer relay between TPE groups and DOX units was interrupted and the "silenced" fluorescence was wakened up, thus realizing in situ visualization of the drug release via the location and magnitude of the energy transfer-dependent fluorescence variation. In vitro experiments proved that the released DOX from DOX-loaded SNPs could suppress cell growth against HeLa cells, which was realized by the

DOI: 10.1021/acsami.7b16734
ACS Appl. Mater. Interfaces 2017, 9, 44392−44401

interruption of the host−guest inclusion complex in the intracellular reducing environment of cancer cells. Furthermore, in vivo investigations demonstrated that these DOX-loaded SNPs were highly accumulated in tumor tissues with the help of the EPR effect and owned a prolonged blood circulation time than DOX·HCl. The chemical design of the cucurbit[8]uril-based amphiphilic supramolecular brush copolymer thus provides an attractive strategy to overcome both the physiological and pathological barriers and increases intratumoral accumulation and permeability of drugs for improved cancer therapeutic efficacy. This work provides a novel strategy to fabricate smart supramolecular nanomedicines with tumor specific responsiveness, showing promising potentials in clinical translation.

4. EXPERIMENTAL SECTION

4.1. Materials and Methods. Cucurbit[8]uril (CB[8]), mPEG-OH (molecular weight: 2000), and other used reagents were bought commercially. Solvents were used directly or after the drying step on the basis of the procedures represented in the literature. PTPE was prepared in line with literature procedures.[69] ^{1}H NMR was scanned on a Bruker AVANCE III-400 spectrometer with an internal standard tetramethylsilane. UV−vis−NIR spectra were measured on a Shimadzu UV-2550 spectrophotometer. Molecular weights and their distributions were identified via gel permeation chromatography (GPC) equipped with a Waters 1515 pump and a Waters 1515 differential refractive index detector (detector temperature is 30 °C); H_2O was employed as the eluent. The fluorescence spectrum experiments were measured on an RF-5301 spectrofluorophotometer (Shimadzu Corporation, Japan). TEM experiments were conducted on a HT-7700 instrument. The cell images were taken by CLSM with a 100× oil immersion lens (Radiance 2100, Bio-Rad). Flow cytometry measurements were conducted using an FACSCalibur flow cytometer (BD FACSCalibur).

4.2. Synthesis of PEG-OTs. To a solution of mPEG-OH (250 g, 125 mmol) in dichloromethane (1000 mL) containing 50.0 mL triethylamine (TEA), paratoluenesulfonylchloride (47.8 g, 250 mmol) was added under the atmosphere of nitrogen. The solution was stirred for 24 h at room temperature. After removal of the organic solvent and purification by column chromatography, the product of PEG-OTs was obtained (white solid, 200 g, 74%).

4.3. Synthesis of PEG-Np. To a solution of PEG-OTs (22.0 g, 10.0 mmol) in CH_3CN (200 mL), K_2CO_3 (13.9 g, 100 mmol) and 2-naphthol (2.88 g, 20 mmol) were gradually added under a nitrogen atmosphere. The solution was refluxed in an oil bath for 24 h. After filtration, removal of the organic solvent, and purification by column chromatography, the product of PEG-Np was obtained (white solid, 18.3 g, 85.0%).

4.4. TEM and DLS Preparations. The morphology of the SNPs was studied by TEM. TEM specimens were prepared by dropping the solution of SNPs onto a treated copper net. The corresponding sample was left to stay overnight and filtered with a 2 μm filter membrane before DLS measurements.

4.5. Preparation of DOX-Loading SNPs. PTPE (17.0 mg) was resolved in 1.0 mL THF, and DOX·HCl (20.0 mg) was resolved in 1.0 mL water in the presence of TEA. Then, the THF and water solutions were dropwisely added into the 2.0 mL aqueous solution in which CB[8] (20.0 mg) and PEG-Np (32.0 mg) were added. After stirring for 24 h in the dark environment, the resulting solution was dialyzed in the deionized water until the unencapsulated DOX was totally removed.

4.6. Controlled Release Studies. The DOX release from the DOX-loaded SNPs in a reduction environment was first studied. The DOX-loaded SNPs (5.00 mg) was dissolved in 2.0 mL phosphate buffer solutions with different concentrations of $Na_2S_2O_4$ and then poured into the dialysis bags (8−14 kDa). The dialysis processed with a frequency of 100 rpm at 37 °C. At the specified time intervals, 1.0 mL sample was taken out from the 25.0 mL solution out of the dialysis bag for UV detection and was then put back into the original system. The UV absorption was measured under the 480 nm. On the basis of the standard curve, the DOX concentrations were calculated.

The DOX release was also studied in different pH buffer solutions. The DOX-loaded SNPs (5.00 mg) were resolved in 2.0 mL phosphate buffers with different pH values and then poured into the dialysis bags (8−14 kDa). The dialysis processed with a frequency of 100 rpm at 37 °C. At the specified time intervals, 1.0 mL sample was taken out from the 25.0 mL solution out of the dialysis bag for UV detection and was then put back into the original system. The UV absorption was measured under the 480 nm. On the basis of the standard curve, the DOX concentrations were calculated.

4.7. Cytotoxicity Assessment. The cytotoxicity tests of DOX·HCl, CB[8]⊃(PEG-Np·PTPE), and DOX-loaded SNPs were evaluated using the MTT assay. HeLa cells were planted in 96-well plates, and the cell density was 8×10^3 cells/well. After overnight adhesion, the serum-containing culture medium was replaced with the serum-free culture medium, which contained various concentrations of DOX·HCl, CB[8]⊃(PEG-Np·PTPE) and DOX-loaded SNPs. After 24 or 48 h incubation, the medium was discarded and HeLa cells were washed using PBS three times. The HeLa cells were then incubated in 100 μL Dulbecco's modified Eagle's medium (DMEM) medium which contained 0.5 mg/mL MTT for another 4 h. After this, 100 μL dimethyl sulfoxide was used to dissolve the formed formazan crystal. Eventually, the data were acquired by using a scanning spectrophotometer (model 550, Bio-Rad) at a wavelength of 570 nm.

4.8. Cellular Uptake Evaluation. HeLa cells were planted in six-well plates, and the cell density was 2×10^5 cells/well. After 24 h incubation, the DOX-loaded SNPs in fresh DMEM medium (the concentration of DOX was 5.00 μM) were added and the HeLa cells were incubated for several specific time intervals, respectively. At last, the cells were trypsinized and resuspended in PBS (0.5 mL). Flow cytometry measurements were conducted using an FACSCalibur flow cytometer (BD FACSCalibur). The mean fluorescence signal was determined by counting 10 000 events.

For confocal imaging, the tested cells were first seeded on the glass slides with a cell density of 1×10^5 mL^{-1}. After overnight adhesion, the cells were cultured with DOX-loaded SNPs at 37 °C for several specific time intervals, respectively. Then, the cells were fixed by fresh 4.0% formaldehyde solution for 15 min at room temperature. The images were photographed using an LSM-510 confocal laser scanning microscope (Radiance 2100, Bio-Rad).

4.9. Tumor Models. Female Balb/c nude mice (4 weeks old, ∼20 g) were bought from Zhejiang Academy of Medical Sciences and fed in the aseptic condition under 24 °C. Throughout the whole experiments, all the operations involving animals were authorized by the Zhejiang University Animal Care and Use Committee. The female nude mice were injected 100 μL cell suspension with a cell density of 8×10^7 mL^{-1} in the right flank region. The tumors were permitted to grow up to ∼100 mm^3 before experimentation. According to the formula: (tumor length) × (tumor width)^2/2, the tumor volume (V) was calculated (V_0 refers to the initial tumor volume).

4.10. Pharmacokinetics. For pharmacokinetic studies, the nude mice were divided into two groups randomly (n = 3). Free DOX·HCl and DOX-loaded SNPs formulations were injected into the tail vein (DOX concentration: 5.00 mg/kg). The samples of blood (0.5 mL) were collected from the eye socket at the specific time intervals. After centrifugation for 15 min at 3000 rpm, the plasma was obtained and the quantity of DOX in it was analyzed by the UV detection.

4.11. In Vivo Fluorescence Imaging. When the tumor volume reached up to 100 mm^3, the mice were injected with DOX·HCl or DOX-loaded SNPs via the tail vein. Whole-body optical imaging was conducted on the IVIS Kinetic imaging system with a excitation filter of 430 nm and a emission filter of 620 nm (Caliper Life Sciences, Hopkinton, MA).

4.12. Evaluation of the Antitumor Effect. The nude mice were randomly allocated into three treatment groups (n = 7). When the mean tumor volume grew up to 100 mm^3, the data was set as day 0. Mice were, respectively, administered with PBS, DOX·HCl, and DOX-loaded SNPs via the tail vein every 3 days (the dosage of DOX was

DOI: 10.1021/acsami.7b16734
ACS Appl. Mater. Interfaces 2017, 9, 44392−44401

5.00 mg/kg). Meanwhile, the body weight and tumor volume of mice were also measured every 3 days. The tumor inhibition study was stopped on the 16th day, and the number of injections was five.

4.13. Tissue Immunohistological Evaluation. After a series of pretreatment steps in line with the standard protocol, the samples of heart, liver, spleen, lung, kidney, and tumor tissues were stained with hematoxylin and eosin (H&E) for the histological assay. For analysis of cell proliferation, the sections were incubated with antiKi67 antibody (1:25, ab28364, Abcam, United Kingdom) and then incubated with the secondary antibody of a Rb IgG (H+L)/HRP (ZB-2301, ZSGB-BIO, China) in accordance with the operating manual. The method of TUNEL was used to detect the apoptosis of in vivo tumor cells after different treatments.

■ ASSOCIATED CONTENT

Supporting Information

The Supporting Information is available free of charge on the ACS Publications website at DOI: 10.1021/acsami.7b16734.

Synthetic route to PEG-Np; ^{1}H NMR spectra and GPC characterization data; UV−vis and fluorescence spectra; cytotoxicity evaluations; TEM and DLS characterization data; in vivo and ex vivo imaging; and photographs of the mice before and after chemotherapy (PDF)

■ AUTHOR INFORMATION

Corresponding Authors

*E-mail: guocan.yu@nih.gov (G.Y.).
*E-mail: tangguping@zju.edu.cn (G.T.).
*E-mail: shawn.chen@nih.gov (X.C.).

ORCID

Guping Tang: 0000-0003-3256-740X
Xiaoyuan Chen: 0000-0002-9622-0870

Author Contributions

D.W., Y.L., and J.Y. contributed equally. The paper was written through contributions of all authors. All authors have given approval to the final version of the paper.

Notes

The authors declare no competing financial interest.

■ ACKNOWLEDGMENTS

This work was supported by the National Natural Science Foundation of China (21434005, 91527301, and 51573161), the National Basic Research Program (2014CB931900), the Intramural Research Program of the National Institute of Biomedical Imaging and Bioengineering, National Institutes of Health, and the Fundamental Research Funds for the Central Universities and Open Project of State Key Laboratory of Supramolecular Structure and Materials.

■ REFERENCES

(1) Cabral, H.; Matsumoto, Y.; Mizuno, K.; Chen, Q.; Murakami, M.; Kimura, M.; Terada, Y.; Kano, M. R.; Miyazono, K.; Uesaka, M.; Nishiyama, N.; Kataoka, K. Accumulation of Sub-100 nm Polymeric Micelles in Poorly Permeable Tumours Depends on Size. *Nat. Nanotechnol.* **2011**, *6*, 815−823.

(2) Devadasu, V. R.; Bhardwaj, V.; Kumar, M. N. V. R. Can Controversial Nanotechnology Promise Drug Delivery? *Chem. Rev.* **2013**, *113*, 1686−1735.

(3) Veiseh, O.; Tang, B. C.; Whitehead, K. A.; Anderson, D. G.; Langer, R. Managing Diabetes with Nanomedicine: Challenges and Opportunities. *Nat. Rev. Drug Discovery* **2015**, *14*, 45−57.

(4) Min, Y.; Caster, J. M.; Eblan, M. J.; Wang, A. Z. Clinical Translation of Nanomedicine. *Chem. Rev.* **2015**, *115*, 11147−11190.

(5) Doane, T. L.; Burda, C. The Unique Role of Nanoparticles in Nanomedicine: Imaging, Drug Delivery and Therapy. *Chem. Soc. Rev.* **2012**, *41*, 2885−2911.

(6) Mura, S.; Nicolas, J.; Couvreur, P. Stimuli-Responsive Nanocarriers for Drug Delivery. *Nat. Mater.* **2013**, *12*, 991−1003.

(7) Blanco, E.; Shen, H.; Ferrari, M. Principles of Nanoparticle Design for Overcoming Biological Barriers to Drug Delivery. *Nat. Biotechnol.* **2015**, *33*, 941−951.

(8) Huynh, E.; Leung, B. Y. C.; Helfield, B. L.; Shakiba, M.; Gandier, J.-A.; Jin, C. S.; Master, E. R.; Wilson, B. C.; Goertz, D. E.; Zheng, G. In Situ Conversion of Porphyrin Microbubbles to Nanoparticles for Multimodality Imaging. *Nat. Nanotechnol.* **2015**, *10*, 325−332.

(9) Du, J.-Z.; Du, X.-J.; Mao, C.-Q.; Wang, J. Tailor-Made Dual pH-Sensitive Polymer−Doxorubicin Nanoparticles for Efficient Anticancer Drug Delivery. *J. Am. Chem. Soc.* **2011**, *133*, 17560−17563.

(10) Hubbell, J. A.; Chilkoti, A. Nanomaterials for Drug Delivery. *Science* **2012**, *337*, 303−305.

(11) Kelley, E. G.; Albert, J. N. L.; Sullivan, M. O.; Epps, T. H., 3rd Stimuli-Responsive Copolymer Solution and Surface Assemblies for Biomedical Applications. *Chem. Soc. Rev.* **2013**, *42*, 7057−7071.

(12) Hu, C.-M. J.; Fang, R. H.; Luk, B. T.; Zhang, L. Nanoparticle-Detained Toxins for Safe and Effective Vaccination. *Nat. Nanotechnol.* **2013**, *8*, 933−938.

(13) Torchilin, V. P. Recent Advances with Liposomes as Pharmaceutical Carriers. *Nat. Rev. Drug Discovery* **2005**, *4*, 145−160.

(14) Pattni, B. S.; Chupin, V. V.; Torchilin, V. P. New Developments in Liposomal Drug Delivery. *Chem. Rev.* **2015**, *115*, 10938−10966.

(15) Robin, M. P.; Mabire, A. B.; Damborsky, J. C.; Thom, E. S.; Winzer-Serhan, U. H.; Raymond, J. E.; O'Reilly, R. K. New Functional Handle for Use as a Self-Reporting Contrast and Delivery Agent in Nanomedicine. *J. Am. Chem. Soc.* **2013**, *135*, 9518−9524.

(16) Yao, J.; Yang, M.; Duan, Y. Chemistry, Biology, and Medicine of Fluorescent Nanomaterials and Related Systems: New Insights into Biosensing, Bioimaging, Genomics, Diagnostics, and Therapy. *Chem. Rev.* **2014**, *114*, 6130−6178.

(17) Wang, Y.; Zhou, K.; Huang, G.; Hensley, C.; Huang, X.; Ma, X.; Zhao, T.; Sumer, B. D.; DeBerardinis, R. J.; Gao, J. A Nanoparticle-Based Strategy for the Imaging of a Broad Range of Tumours by Nonlinear Amplification of Microenvironment Signals. *Nat. Mater.* **2014**, *13*, 204−212.

(18) Elsabahy, M.; Heo, G. S.; Lim, S.-M.; Sun, G.; Wooley, K. L. Polymeric Nanostructures for Imaging and Therapy. *Chem. Rev.* **2015**, *115*, 10967−11011.

(19) Park, J.; Wrzesinski, S. H.; Stern, E.; Look, M.; Criscione, J.; Ragheb, R.; Jay, S. M.; Demento, S. L.; Agawu, A.; Licona Limon, P.; Ferrandino, A. F.; Gonzalez, D.; Habermann, A.; Flavell, R. A.; Fahmy, T. M. Combination Delivery of TGF-β Inhibitor and IL-2 by Nanoscale Liposomal Polymeric Gels Enhances Tumour Immunotherapy. *Nat. Mater.* **2012**, *11*, 895−905.

(20) Elsabahy, M.; Wooley, K. L. Data Mining as a Guide for the Construction of Cross-Linked Nanoparticles with Low Immunotoxicity via Control of Polymer Chemistry and Supramolecular Assembly. *Acc. Chem. Res.* **2015**, *48*, 1620−1630.

(21) Dong, R.; Zhou, Y.; Huang, X.; Zhu, X.; Lu, Y.; Shen, J. Functional Supramolecular Polymers for Biomedical Applications. *Adv. Mater.* **2015**, *27*, 498−526.

(22) Webber, M. J.; Appel, E. A.; Meijer, E. W.; Langer, R. Supramolecular Biomaterials. *Nat. Mater.* **2016**, *15*, 13−26.

(23) Tu, Y.; Peng, F.; Adawy, A.; Men, Y.; Abdelmohsen, L. K. E. A.; Wilson, D. A. Mimicking the Cell: Bio-Inspired Functions of Supramolecular Assemblies. *Chem. Rev.* **2016**, *116*, 2023−2078.

(24) Yoon, D.-W.; Gross, D. E.; Lynch, V. M.; Sessler, J. L.; Hay, B. P.; Lee, C.-H. Benzene-, Pyrrole-, and Furan-Containing Diametrically Strapped Calix[4]pyrroles-An Experimental and Theoretical Study of Hydrogen-Bonding Effects in Chloride Anion Recognition. *Angew. Chem., Int. Ed.* **2008**, *47*, 5038−5042.

(25) Yan, Q.; Zhou, R.; Fu, C.; Zhang, H.; Yin, Y.; Yuan, J. CO_2-Responsive Polymeric Vesicles that Breathe. *Angew. Chem., Int. Ed.* **2011**, *50*, 4923−4927.

(26) Ji, X.; Dong, S.; Wei, P.; Xia, D.; Huang, F. A Novel Diblock Copolymer with a Supramolecular Polymer Block and a Traditional Polymer Block: Preparation, Controllable Self-Assembly in Water, and Application in Controlled Release. *Adv. Mater.* **2013**, *25*, 5725−5729.
(27) Talotta, C.; Gaeta, C.; Qi, Z.; Schalley, C. A.; Neri, P. Pseudorotaxanes with Self-Sorted Sequence and Stereochemical Orientation. *Angew. Chem., Int. Ed.* **2013**, *52*, 7437−7441.
(28) Rauwald, U.; Scherman, O. A. Supramolecular Block Copolymers with Cucurbit[8]uril in Water. *Angew. Chem., Int. Ed.* **2008**, *47*, 3950−3953.
(29) Zhang, J.; Ma, P. X. Polymeric Core-Shell Assemblies Mediated by Host-Guest Interactions: Versatile Nanocarriers for Drug Delivery. *Angew. Chem., Int. Ed.* **2009**, *48*, 964−968.
(30) Quan, C.-Y.; Chen, J.-X.; Wang, H.-Y.; Li, C.; Chang, C.; Zhang, X.-Z.; Zhuo, R.-X. Core−Shell Nanosized Assemblies Mediated by the $\alpha-\beta$ Cyclodextrin Dimer with a Tumor-Triggered Targeting Property. *ACS Nano* **2010**, *4*, 4211−4219.
(31) Duan, Q.; Cao, Y.; Li, Y.; Hu, X.; Xiao, T.; Lin, C.; Pan, Y.; Wang, L. pH-Responsive Supramolecular Vesicles Based on Water-Soluble Pillar[6]arene and Ferrocene Derivative for Drug Delivery. *J. Am. Chem. Soc.* **2013**, *135*, 10542−10549.
(32) Xue, X.; Zhao, Y.; Dai, L.; Zhang, X.; Hao, X.; Zhang, C.; Huo, S.; Liu, J.; Liu, C.; Kumar, A.; Chen, W.-Q.; Zou, G.; Liang, X.-J. Spatiotemporal Drug Release Visualized Through a Drug Delivery System with Tunable Aggregation-Induced Emission. *Adv. Mater.* **2014**, *26*, 712−717.
(33) Zhang, C.; Jin, S.; Li, S.; Xue, X.; Liu, J.; Huang, Y.; Jiang, Y.; Chen, W.-Q.; Zou, G.; Liang, X.-J. Imaging Intracellular Anticancer Drug Delivery by Self-Assembly Micelles with Aggregation-Induced Emission (AIE Micelles). *ACS Appl. Mater. Interfaces* **2014**, *6*, 5212−5220.
(34) Xue, X.; Jin, S.; Zhang, C.; Yang, K.; Huo, S.; Chen, F.; Zou, G.; Liang, X.-J. Probe-Inspired Nano-Prodrug with Dual-Color Fluorogenic Property Reveals Spatiotemporal Drug Release in Living Cells. *ACS Nano* **2015**, *9*, 2729−2739.
(35) Yu, G.; Wu, D.; Li, Y.; Zhang, Z.; Shao, L.; Zhou, J.; Hu, Q.; Tang, G.; Huang, F. A Pillar[5]arene-Based [2]Rotaxane Lights up Mitochondria. *Chem. Sci.* **2016**, *7*, 3017−3024.
(36) Kim, K.; Kim, D.; Lee, J. W.; Ko, Y. H.; Kim, K. Growth of Poly(pseudorotaxane) on Gold Using Host-Stabilized Charge-Transfer Interaction. *Chem. Commun.* **2004**, 848−849.
(37) Lagona, J.; Mukhopadhyay, P.; Chakrabarti, S.; Isaacs, L. The Cucurbit[n]uril Family. *Angew. Chem., Int. Ed.* **2005**, *44*, 4844−4870.
(38) Bush, M. E.; Bouley, N. D.; Urbach, A. R. Charge-Mediated Recognition of N-Terminal Tryptophan in Aqueous Solution by a Synthetic Host. *J. Am. Chem. Soc.* **2005**, *127*, 14511−14517.
(39) Kim, H.-J.; Heo, J.; Jeon, W. S.; Lee, E.; Kim, J.; Sakamoto, S.; Yamaguchi, K.; Kim, K. Selective Inclusion of a Hetero-Guest Pair in a Molecular Host: Formation of Stable Charge-Transfer Complexes in Cucurbit[8]uril. *Angew. Chem., Int. Ed.* **2001**, *40*, 1526−1529.
(40) Liu, Y.; Yu, Y.; Gao, J.; Wang, Z.; Zhang, X. Water-Soluble Supramolecular Polymerization Driven by Multiple Host-Stabilized Charge-Transfer Interactions. *Angew. Chem., Int. Ed.* **2010**, *49*, 6576−6579.
(41) Barrow, S. J.; Kasera, S.; Rowland, M. J.; del Barrio, J.; Scherman, O. A. Cucurbituril-Based Molecular Recognition. *Chem. Rev.* **2015**, *115*, 12320−12406.
(42) Wang, W.; Kaifer, A. E. Electrochemical Switching and Size Selection in Cucurbit[8]uril-Mediated Dendrimer Self-Assembly. *Angew. Chem., Int. Ed.* **2006**, *45*, 7042−7046.
(43) Tan, C. S. Y.; del Barrio, J.; Liu, J.; Scherman, O. A. Supramolecular Polymer Networks Based on Cucurbit[8]uril Host−Guest Interactions as Aqueous Photo-Rheological Fluids. *Polym. Chem.* **2015**, *6*, 7652−7657.
(44) Hu, C.; Lan, Y.; West, K. R.; Scherman, O. A. Cucurbit[8]uril-Regulated Nanopatterning of Binary Polymer Brushes via Colloidal Templating. *Adv. Mater.* **2015**, *27*, 7957−7962.
(45) Yu, G.; Zhou, X.; Zhang, Z.; Han, C.; Mao, Z.; Gao, C.; Huang, F. Pillar[6]arene/Paraquat Molecular Recognition in Water: High Binding Strength, pH-Responsiveness, and Application in Controllable Self-Assembly, Controlled Release, and Treatment of Paraquat Poisoning. *J. Am. Chem. Soc.* **2012**, *134*, 19489−19497.
(46) Ko, Y. H.; Kim, K.; Kang, J.-K.; Chun, H.; Lee, J. W.; Sakamoto, S.; Yamaguchi, K.; Fettinger, J. C.; Kim, K. Designed Self-Assembly of Molecular Necklaces Using Host-Stabilized Charge-Transfer Interactions. *J. Am. Chem. Soc.* **2004**, *126*, 1932−1933.
(47) Barrow, S. J.; Kasera, S.; Rowland, M. J.; del Barrio, J.; Scherman, O. A. Cucurbituril-Based Molecular Recognition. *Chem. Rev.* **2015**, *115*, 12320−12406.
(48) Yu, Z.; Zheng, Y.; Parker, R. M.; Lan, Y.; Wu, Y.; Coulston, R. J.; Zhang, J.; Scherman, O. A.; Abell, C. Microfluidic Droplet-Facilitated Hierarchical Assembly for Dual Cargo Loading and Synergistic Delivery. *ACS Appl. Mater. Interfaces* **2016**, *8*, 8811−8820.
(49) Dinis-Oliveira, R. J.; Sousa, C.; Remião, F.; Duarte, J. A.; Navarro, A. S.; Bastos, M. L.; Carvalho, F. Full Survival of Paraquat-Exposed Rats after Treatment With Sodium Salicylate. *Free Radical Biol. Med.* **2007**, *42*, 1017−1028.
(50) Ni, X.-L.; Xiao, X.; Cong, H.; Zhu, Q.-J.; Xue, S.-F.; Tao, Z. Self-Assemblies Based on the "Outer-Surface Interactions" of Cucurbit[n]urils: New Opportunities for Supramolecular Architectures and Materials. *Acc. Chem. Res.* **2014**, *47*, 1386−1395.
(51) Isaacs, L. Stimuli Responsive Systems Constructed Using Cucurbit[n]uril-Type Molecular Containers. *Acc. Chem. Res.* **2014**, *47*, 2052−2062.
(52) Kaifer, A. E. Toward Reversible Control of Cucurbit[n]uril Complexes. *Acc. Chem. Res.* **2014**, *47*, 2160−2167.
(53) Li, Q.-L.; Sun, Y.; Sun, Y.-L.; Wen, J.; Zhou, Y.; Bing, Q.-M.; Isaacs, L. D.; Jin, Y.; Gao, H.; Yang, Y.-W. Mesoporous Silica Nanoparticles Coated by Layer-by-Layer Self-assembly Using Cucurbit[7]uril for in Vitro and in Vivo Anticancer Drug Release. *Chem. Mater.* **2014**, *26*, 6418−6431.
(54) Han, X.; Liu, D.-E.; Wang, T.; Lu, H.; Ma, J.; Chen, Q.; Gao, H. Aggregation-induced-emissive Molecule Incorporated into Polymeric Nanoparticulate as FRET Donor for Observing Doxorubicin Delivery. *ACS Appl. Mater. Interfaces* **2015**, *7*, 23760−23766.
(55) Li, Q.; Wu, Y.; Lu, H.; Wu, X.; Chen, S.; Song, N.; Yang, Y.-W.; Gao, H. Construction of Supramolecular Nanoassembly for Responsive Bacterial Elimination and Effective Bacterial Detection. *ACS Appl. Mater. Interfaces* **2017**, *9*, 10180−10189.
(56) Barrett, E. S.; Dale, T. J.; Rebek, J. Self-Assembly Dynamics of a Cylindrical Capsule Monitored by Fluorescence Resonance Energy Transfer. *J. Am. Chem. Soc.* **2007**, *129*, 8818−8824.
(57) Prevo, B.; Peterman, E. J. G. Förster Resonance Energy Transfer and Kinesin Motor Proteins. *Chem. Soc. Rev.* **2014**, *43*, 1144−1155.
(58) Yuan, H.; Qi, J.; Xing, C.; An, H.; Niu, R.; Zhan, Y.; Fan, Y.; Yan, W.; Li, R.; Wang, B.; Wang, S. Graphene-Oxide-Conjugated Polymer Hybrid Materials for Calmodulin Sensing by Using FRET Strategy. *Adv. Funct. Mater.* **2015**, *25*, 4412−4418.
(59) Peng, H.-Q.; Niu, L.-Y.; Chen, Y.-Z.; Wu, L.-Z.; Tung, C.-H.; Yang, Q.-Z. Biological Applications of Supramolecular Assemblies Designed for Excitation Energy Transfer. *Chem. Rev.* **2015**, *115*, 7502−7542.
(60) Samanta, S. K.; Moncelet, D.; Briken, V.; Isaacs, L. Metal−Organic Polyhedron Capped with Cucurbit[8]uril Delivers Doxorubicin to Cancer Cells. *J. Am. Chem. Soc.* **2016**, *138*, 14488−14496.
(61) Liu, W.; Samanta, S. K.; Smith, B. D.; Isaacs, L. Synthetic mimics of biotin/(strept)avidin. *Chem. Soc. Rev.* **2017**, *46*, 2391−2403.
(62) Huang, P.; Lin, J.; Li, W.; Rong, P.; Wang, Z.; Wang, S.; Wang, X.; Sun, X.; Aronova, M.; Niu, G.; Leapman, R. D.; Nie, Z.; Chen, X. Biodegradable Gold Nanovesicles with an Ultrastrong Plasmonic Coupling Effect for Photoacoustic Imaging and Photothermal Therapy. *Angew. Chem., Int. Ed.* **2013**, *52*, 13958−13964.
(63) Hu, X.; Hu, J.; Tian, J.; Ge, Z.; Zhang, G.; Luo, K.; Liu, S. Polyprodrug Amphiphiles: Hierarchical Assemblies for Shape-Regulated Cellular Internalization, Trafficking, and Drug Delivery. *J. Am. Chem. Soc.* **2013**, *135*, 17617−17629.
(64) Wang, Y.; Lin, Y.-X.; Qiao, Z.-Y.; An, H.-W.; Qiao, S.-L.; Wang, L.; Rajapaksha, R. P. Y. J.; Wang, H. Self-Assembled Autophagy-

DOI: 10.1021/acsami.7b16734
ACS Appl. Mater. Interfaces 2017, 9, 44392−44401

Inducing Polymeric Nanoparticles for Breast Cancer Interference In-Vivo. *Adv. Mater.* **2015**, *27*, 2627−2634.
(65) Han, H.; Wang, H.; Chen, Y.; Li, Z.; Wang, Y.; Jin, Q.; Ji, J. Theranostic Reduction-Sensitive Gemcitabine Prodrug Micelles for Near-Infrared Imaging and Pancreatic Cancer Therapy. *Nanoscale* **2016**, *8*, 283−291.
(66) Kim, H. J.; Takemoto, H.; Yi, Y.; Zheng, M.; Maeda, Y.; Chaya, H.; Hayashi, K.; Mi, P.; Pittella, F.; Christie, R. J.; Toh, K.; Matsumoto, Y.; Nishiyama, N.; Miyata, K.; Kataoka, K. Precise Engineering of siRNA Delivery Vehicles to Tumors Using Polyion Complexes and Gold Nanoparticles. *ACS Nano* **2014**, *8*, 8979−8991.
(67) Tian, Y.; Jiang, X.; Chen, X.; Shao, Z.; Yang, W. Doxorubicin-Loaded Magnetic Silk Fibroin Nanoparticles for Targeted Therapy of Multidrug-Resistant Cancer. *Adv. Mater.* **2014**, *26*, 7393−7398.
(68) Huang, P.; Wang, W.; Zhou, J.; Zhao, F.; Zhang, Y.; Liu, J.; Liu, J.; Dong, A.; Kong, D.; Zhang, J. Amphiphilic Polyelectrolyte/Prodrug Nanoparticles Constructed by Synergetic Electrostatic and Hydrophobic Interactions with Cooperative pH-Sensitivity for Controlled Doxorubicin Delivery. *ACS Appl. Mater. Interfaces* **2015**, *7*, 6340−6350.
(69) Yu, G.; Zhao, R.; Wu, D.; Zhang, F.; Shao, L.; Zhou, J.; Yang, J.; Tang, G.; Chen, X.; Huang, F. Pillar[5]arene-based amphiphilic supramolecular brush copolymers: fabrication, controllable self-assembly and application in self-imaging targeted drug delivery. *Polym. Chem.* **2016**, *7*, 6178−6188.

DOI: 10.1021/acsami.7b16734
ACS Appl. Mater. Interfaces 2017, 9, 44392−44401